HHS Public Access

Author manuscript

Neuron. Author manuscript; available in PMC 2021 October 22.

Published in final edited form as:

Neuron. 2008 August 14; 59(3): 425–438. doi:10.1016/j.neuron.2008.07.018.

Architecture and activity-mediated refinement of axonal projections from a mosaic of genetically identified retinal ganglion cells

Andrew D. Huberman[1], **Mihai Manu**[1], **Selina Koch**[2], **Michael W. Susman**[1], **Amanda Brosius Lutz**[1], **Erik M. Ullian**[2], **Stephen A. Baccus**[1,#], **Ben A. Barres**[1,#]

[1]Department of Neurobiology, Fairchild Science Building D235, Stanford University School of Medicine, Palo Alto, CA 94305

[2]Department of Ophthalmology and Physiology, University of California, San Francisco, CA 94117

SUMMARY

Our understanding of how mammalian sensory circuits are organized and develop has long been hindered by the lack of genetic markers of neurons with discrete functions. Here we report a transgenic mouse selectively expressing GFP in a complete mosaic of transient OFF-α retinal ganglion cells (tOFF-αRGCs). This enabled us to relate the mosaic spacing, dendritic anatomy, and electrophysiology of these RGCs to their complete map of projections in the brain. We find that tOFF-αRGCs project exclusively to the superior colliculus (SC) and dorsal lateral geniculate nucleus and are restricted to a specific laminar depth within each of these targets. The axons of tOFF-αRGC are also organized into columns in the SC. Both laminar and columnar specificity develop through axon refinement. Disruption of cholinergic retinal waves prevents the emergence of columnar- but not laminar-specific tOFF-αRGC connections. Our findings reveal that in a genetically identified sensory map, spontaneous activity promotes synaptic specificity by segregating axons arising from RGCs of the same subtype.

INTRODUCTION

The transmission of topographically organized sensory information poses a substantial problem for central nervous system (CNS) development. Sensory axons must travel long distances to reach their targets, yet still maintain their local relationships so that the map is preserved. The current model is that molecular guidance cues steer axons through a series of decision points leading to their targets and then spontaneous neural activity and guidance cues refine those projections into an orderly, continuous topographic map (McLaughlin and O'Leary, 2005; Luo and Flanagan, 2007). Within this general model, however, several

To whom correspondence should be addressed: Andrew D. Huberman, Stanford University School of Medicine, Department of Neurobiology, Fairchild Science Building, D231, 299 Campus Drive, Stanford, CA 94305-5125, Tel: (650) 498-7901; Fax: (650) 725-3958, adh1@stanford.edu.

[#]Co-senior authors

aspects of the construction of mammalian sensory circuits remain poorly understood. For instance, a hallmark feature of sensory pathways is their parallel organization: different neurons respond to and convey qualitatively distinct information about a given sensory modality (Callaway, 2005). How axons carrying distinct types of sensory information are organized within continuous topographic maps and how those projections develop is unclear. A major obstacle for studying this aspect of circuit wiring- often called 'synaptic specificity' (Benson et al., 2001) is a lack of genetic markers that ensure stable, selective and complete labeling of functionally identified classes of neurons in mammals. Several basic and important questions related to development of sensory circuits in the mammalian CNS therefore remain unresolved. For example, it is unknown whether emergence of synaptic specificity involves refinement of initially inaccurate projections or whether functionally specific circuits are accurately formed from the outset, as they are in the invertebrate nervous system (Meinertzhagen and Hansen, 1993). A related question is whether neural activity contributes to the emergence of synaptic specificity.

In principle, the connections associated with different types of retinal ganglion cells (RGC) would be ideal for exploring the emergence of synaptic specificity in the mammalian CNS. Conventional dye labeling and electrophysiological recording techniques indicate that there are approximately two dozen anatomically and physiologically distinct subtypes of RGCs (reviewed in: Wässle, 2004; Berson, 2008). Each RGC subtype receives qualitatively distinct information about the content of the visual scene by virtue of its laminar-specific dendritic connections with bipolar and amacrine cells in the inner plexiform layer (IPL) (Roska and Werblin, 2001) and in turn, conveys that information to the brain by sending axonal projections to specific retinorecipient nuclei (Berson, 2008). Despite extensive study of the physiology and connectivity associated with different RGCs, the total number of functionally-distinct RGC subtypes and the complete wiring diagram corresponding to any one individual RGC subtype still remains unclear (Sun et al., 2002; Kong et al., 2005; Berson, 2008).

In order to study the organization and development of neural circuitry corresponding to distinct RGC subtypes, we screened a library of BAC transgenic mice with GFP expressed under the control of different promoters (Gong et al., 2003). Our goal was to identify mouse lines in which, i) GFP is expressed in a mosaic of RGCs throughout the retina- because mosaic spacing suggests that cell population is comprised of a functionally homogeneous RGC subtype (Wässle, 2004) and ii) there are few or no cells expressing GFP in retinorecipient brain areas, so the organization of axonal projections from the GFP-expressing RGCs can be visualized during development and adulthood.

RESULTS

A transgenic mouse with a complete mosaic of one RGC subtype expressing GFP

Calretinin-EGFP mice (CB2-GFP mice) met both criteria of our screen. In the retinas of these mice, GFP is expressed by a population of regularly spaced cells throughout the ganglion cell layer (GCL) (Figure 1A, B, E) (mean=368 ±14 GFP^+ RGCs per retina; n=6 mice). The presence of an axon emanating from each GFP^+ cell confirmed they were RGCs (Figure 1B inset). In addition, as expected for RGCs, all the GFP^+ cells in the RGC

layer degenerated in response to optic nerve transection (data not shown). Every GFP$^+$ RGC stained with the antibody SMI-32 (Figure 1B–D), which recognizes a neurofilament antigen enriched in αRGCs (Peichl, 1991). In addition, the relatively large (~20–25μm) and spherical GFP$^+$ somata resembled mouse αRGCs (Pang et al., 2003; Schubert et al., 2005; Volgyi et al., 2005). In CB2-GFP mice, GFP is also expressed by a population of amacrine cells in the inner nuclear layer (INL) (Figure 1A, E). Based on their morphology and calretinin expression (Lee et al., 1995) we assume those to be AII amacrines, although they may include other amacrine types. In vertical retinal sections (Figure 1E), the GFP$^+$ amacrines in the INL and the regularly spaced GFP$^+$ RGCs (Figure 1E, arrows) were both clearly visible. The somas of GFP$^+$ RGCs formed a highly regular mosaic across the entire retina. This distribution was not random, as cell bodies obeyed a minimum spacing rule, avoiding each other to a distance of approximately 100 μm (Figure 1F). To visualize clearly the dendrites of single cells, we targeted individual GFP$^+$ RGCs with electrodes and filled them with DiI (n=22 RGCs from 5 mice). The dendrites of neighboring GFP$^+$ RGCs tiled the retina with the amount of overlap typical of mouse OFF-αRGCs (Figure 1G) (supplemental figure 1) (Schubert et al., 2005; Volgyi et al., 2005). The DiI fills also revealed that the GFP$^+$ RGCs possessed dendritic features characteristic of mouse OFF-αRGCs (Figure1 G, H) (supplemental figure 1) (Pang et al., 2003; Schubert et al., 2005; Volgyi et al., 2005). We observed that, in every case, the dendrites of the GFP$^+$ RGCs were monostratified at the inner 30–35% depth of the IPL (Figure 1G), within the “OFF” sublaminae (Famiglietti and Kolb, 1976). When the retina was sectioned in the vertical plane and stained for the vesicle acetylcholine transporter (VAChT) (which delineates ON and OFF sublaminae in the IPL) it was apparent that every GFP$^+$ RGC projected its dendrites exclusively into the OFF sublaminae (Figure 1I) (>600 GFP$^+$ RGCs examined from 12 CB2-GFP mice). Collectively, these observations indicate that a mosaic of OFF-αRGCs selectively express GFP in this mouse line.

We next recorded intracellularly from the GFP$^+$ RGCs by visually targeting the cells with a microelectrode under a fluorescence microscope. In response to a flashing visual stimulus, these cells showed transient OFF-type responses, depolarizing and spiking briefly at the offset of a flash (Figure 2A). Visual responses of different GFP$^+$ RGCs were very homogeneous, in that the average of each cell’s flash response was highly correlated with the population average (correlation coefficient $r = 0.93 \pm 0.02$, n=7) (Figure 2B). Further characterization of these cells using a randomly flickering visual stimulus confirmed the transient OFF-type nature of these cells, which showed a biphasic temporal response that peaked at 105 – 121 ms relative to the visual stimulus (n=3) (Figure 2C–D). Taken with our anatomical observations we conclude that a retinotopic mosaic of transient OFF-αRGCs (tOFF-αRGCs) expresses GFP in this mouse line.

A highly organized map of the tOFF-αRGC mosaic in the brain

To determine the connections made by tOFF-αRGCs in the brain we injected cholera toxin beta conjugated to Alexa 594 (CTb-594; red label in Figures 3–8), which labels the axons of all RGCs, into both eyes of CB2-GFP mice and then examined the brain for axons that were both CTb-594$^+$ and GFP$^+$. Of the approximately two-dozen brain regions targeted by RGC axons, tOFF-αRGCs project to only two of these: (1) the superior colliculus (SC), a

midbrain structure involved in sensory-motor integration and (2) the dorsal lateral geniculate nucleus (dLGN), a forebrain structure that filters and relays visual information to primary visual cortex.

The mouse SC receives projections from many different types of RGCs and contains a two-dimensional topographic map of the entire contralateral retina. The dorsal-ventral axis of the retina is mapped along the lateral-medial axis of the SC and the temporal-nasal retinal axis is mapped along the rostral-caudal axis of the SC (Hubel and Dräger, 1976; May, 2005). When the SC is viewed in the coronal plane (Figure 3A) the axons of RGCs can be seen entering the SC deep to the pial surface, in the stratum opticum (SO) and their dense terminal arborizations can be observed in the overlying stratum griseum superficialis (SGS) (Figure 3A). As the main retinorecipient division of the SC, the SGS is divided into lower (lSGS) and upper (uSGS) lamina based on the types of afferent input and postsynaptic cells residing along its depth. A limited number of RGC axons also project to the stratum zonale (SZ), a thin layer located just below the pial margin (May, 2005). We observed that the GFP^+ axons of tOFF-αRGCs terminate in a highly specific and stereotyped manner within the SC. Their axons entered the SC through the SO, along with all other RGC axons, and terminated in the overlying SGS. Within the SGS, however, the GFP^+ arbors of tOFF-αRGCs were faithfully restricted to the lSGS (Figure 3B and C; B' and C'), avoiding the uSGS and SZ entirely. Viewed in the sagittal plane, laminar-specific targeting of tOFF-αRGC projections to the lSGS was also apparent (Figure 3D). When one eye was removed, all GFP^+ axons disappeared from the contralateral SC, indicating that the GFP^+ axons observed in each hemisphere of the SC arise soley from tOFF-αRGCs in the contralateral retina (supplemental figure 2). Retrograde labeling experiments indicated that every GFP^+ tOFF-αRGC projects to the SC (data not shown). Taken with the fact that the GFP^+ axons are restricted to the lSGS across the full lateral-medial (Figure 3B, C) and rostral-caudal (Figure 3D) extent of the SC, we can conclude that every tOFF-αRGC obeys strict laminar specificity of its axonal projection to this target, regardless of its retinotopic position.

Another salient feature of the tOFF-αRGC projecions to the SC was that, within the lSGS, their arbors were regularly spaced to form patches of innervated and non-innervated territory (Figure 3A–D). Based on their regular increased density of projections within the topographic map, we refer to these structures as columns. Retinocollicular projections are known to be organized into columns of alternating right-eye and left-eye RGC input in cats (May, 2005). The GFP^+ columns observed in in the SC of CB2-GFP mice do not relate to eye-specificity, however, because all the GFP^+ axons in the SC originate from the contralateral retina (supplemental figure 2).

We counted ~90 GFP^+ columns per SC hemisphere (88–96 columns; n=6 mice). Given that an entire mosaic of ~370 tOFF-αRGCs expresses GFP and projects to the contralateral SC we could not determine how many tOFF-αRGCs project to each column. In the caudal SC, however, RGC axons were sparse enough that we could observe cases where individual GFP^+ axons bifurcated to terminate in two neighboring, separate columns (supplemental figure 3). Because the degree of retinocollicular convergence varies according to position within the retinotopic map (Drager and Hubel, 1976; Berson, 1988) it is unclear if such

bifurcation is a general rule for all tOFF-αRGCs or is limited to the caudal SC. We observed regularly spaced GFP$^+$ columns across all axes of the SC (Figure 3A–D), indicating that there is a highly organized columnar map corresponding to the mosaic of tOFF-αRGCs within this target.

Unlike the dLGN of carnivores and primates (Callaway, 2005), the rodent dLGN lacks overt laminar cytoarchitecture corresponding to eye-specific inputs or to functionally specialized visual processing streams (Reese, 1988). We were therefore surprised to observe strict laminar specificity of tOFF-αRGC projections to the dLGN. GFP$^+$ axons projected through the lateral third of the dLGN to selectively terminate within the inner/medial portion of the nucleus, where they form a well-demarcated “layer” (Figure 3E–G). Eye removal experiments indicated that the GFP$^+$ axons projecting to the dLGN arose exclusively from the contralateral retina (supplemental figure 2). Given that every GFP$^+$ RGC projects to the SC, the layer-specific tOFF-αRGC projections to the dLGN must be the collaterals of retinocollicular axons. Together, the presence of laminar- and columnar-specific projections to the SC and the laminar-specific projections to dLGN, indicates there is a highly precise brain map associated with the tOFF-αRGC mosaic.

Emergence of laminar and columnar specificity involves axonal refinement

How do the highly specific patterns of axonal connections made by tOFF-αRGCs arise during development? This could occur by a mechanism in which each RGC axon is guided directly and precisely to its proper layer and column/s, as has been described for retinal projections in the fly and in the chick (Meinertzhagen and Hansen, 1993; Inoue and Sanes, 1997). Alternatively, tOFF-αRGC axons could at first project broadly within their targets, and subsequently refine to achieve laminar and columnar specificity, as is the case for retinotopic and eye-specific mapping in mammals (McLaughlin and O’Leary, 2005; Torborg and Feller, 2005). Because tOFF-αRGC projections to the SC exhibit both laminar- and columnar-specificity (Figure 3) and because the SC develops relatively early (Edwards et al., 1986) we examined the development of these features in the retinocollicular pathway.

Studies in mice and hamsters have shown that RGC axons reach the SC slightly before birth and initially overshoot their correct retinotopic termination zone. Between postnatal day 0 (P0) and ~P4, RGC axons retract within the SO, establishing a coarse retinotopic map (McLaughlin and O’Leary, 2005). Subsequently, RGC axons elaborate terminal arbors in the overlying SGS (Sachs et al., 1986). We observed that on P4, the axons of tOFF-αRGCs do not exhibit their mature pattern of laminar or columnar specificity (Figure 4A–C’). While tOFF-αRGC axons tended to arborize in the lSGS and rudimentary columns were evident (Figure 4A–C), it was readily apparent that many GFP$^+$ tOFF-αRGC axons extend across the entire retinorecipient depth of the SC (Figure 4A–C’), a pattern never observed in adulthood (Figure 3). Indeed, on P4, many GFP$^+$ axons projected all the way up to the pial margin of the SC (arrows in Figure 4B’, C’). On P10, by contrast, laminar- and columnar-specificity of tOFF-αRGC retinocollicular projections resembled the adult pattern (Figure 4D–F’). Quantitative analysis confirmed that a significantly greater number of GFP$^+$ axons project to the uSGS and SZ (the upper half of the retinorecipient SC; 0–50% depth from the pial margin) in P4 mice as compared to P10 or adult mice (Figure 4G). There was

also significantly less columnar specificity of tOFF-αRGC retinocollicular projections in P4 mice compared to P10 or adult mice (Figure 4H).

It is unlikely that the lack of laminar and columnar specificity observed in P4 CB2-GFP mice is related to immaturity of the SC layers or to increased numbers of RGCs expressing GFP at this age because development of the retinorecipient SC layers and RGC apoptosis are completed by P4 (Edwards et al., 1986; Farah and Easter, 2005). Indeed, we found that both the thickness of the retinorecipient SC (Figure 4I) and the number of GFP^+ RGCs per retina were indistinguishable between P4, P10 and adult CB2-GFP mice (Figure 4J). Also, as in the adult mouse (supplemental figure 2), the GFP^+ axons observed in the SC of developing CB2-GFP mice arise soley from tOFF-αRGCs in the contralateral retina and not from other sources (supplemental figure 4). We therefore conclude that the development of laminar- and columnar-specific retinocollicular projections involves axonal retraction and refinement. Thus, in addition to any potential mechanisms that direct tOFF-αRGC axons to their correct laminar and columnar positions, there must also be mechanisms in place to remove the incorrect projections made by these RGCs during early postnatal development.

Cholinergic spontaneous retinal activity regulates emergence of columnar specificity

Laminar and columnar specificity of tOFF-αRGC projections to the SC emerges between P4 and P10, which is prior to the onset of vision (Demas et al., 2003). During this period, however, ”waves” of neural activity sweep across the retina, inducing correlated firing of neighboring RGCs (Wong, 1999). Given that P4 to P10 coincides with the presence of cholinergic-mediated retinal waves (Bansal et al., 2000; McLaughlin et al., 2003), we tested the role of that activity on the emergence of laminar- and columnar-specific tOFF-αRGC projections to the SC and the dLGN.

In the first set of experiments, we mated CB2-GFP mice to mice lacking the β2-subunit of the nicotinic acetylcholine receptor (β2nAChR−/−) (Picciotto et al., 1995; Xu et al., 1999) to generate CB2-GFP:β2nAChR−/− mice. β2nAChR−/− mice exhibit significantly altered patterns of RGC bursting during the first 8 days of postnatal life, after which spontaneous and visually evoked RGC activity returns to normal (Bansal et al., 2000; McLaughlin et al., 2003). At P4/5, the degree of laminar- and columnar-specificity in the SC was qualitatively and quantitatively indistinguishable between CB2-GFP:β2nAChR+/+ (WT) mice, CB2-GFP:β2nAChR+/− mice, and CB2-GFP:β2nAChR−/− mice (Figure 5). On P10, however, CB2-GFP:β2nAChR−/− mice exhibited a severely abnormal pattern of tOFF-αRGC projections to the SC (Figure 6A–F). Whereas overall target selection and laminar specificity were normal in the SC (Figure 6A–E) and in the dLGN (Figure 7), there was an obvious reduction in columnar specificity among tOFF-αRGC axons in the SC of CB2-GFP:β2nAChR−/− mice (Figure 6C, D, F).

Remarkably, even though spontaneous retinal activity in β2nAChR−/− mice returns to normal by P8 (Bansal et al., 2000; McLaughlin et al., 2003; Torborg and Feller, 2005) columnar specificity remained severely abnormal in adult CB2-GFP:β2nAChR−/− mice (Figure 6F, I). This shows there is a critical period for columnar segregation of tOFF-αRGC projections that is mediated by β2nAChR-mediated spontaneous retinal activity during the first postnatal week. Importantly, the number of GFP^+ tOFF-αRGCs and the retinorecipient

thickness of the SC were both normal in CB2-GFP:β2nAChR−/− mice (Figure 6G, H). We thus attribute the permanent loss of columnar specificity in CB2-GFP:β2nAChR−/− mice to a lack of β2nAChR-mediated RGC activity and not to altered RGC survival or indirect effects of the mutation on SC cells.

β2nAChR−/− mice lack β2nAChRs throughout the brain, including in the SC where they are normally expressed (Picciotto et al., 1995; Xu et al., 1999). So even though several aspects of RGC axon targeting are normal in CB2-GFP:β2nAChR−/− mice (Figure 6 and 7), the above experiments do not unequivocally determine whether cholinergic spontaneous retinal activity intructs columnar-specific refinement of tOFF-αRGC projections or whether there is a more general requirement for β2nAChRs for columns to develop. To address this, we injected epibatidine (epi), a cholinergic agonist that perturbs spontaneous RGC bursting in the early postnatal retina (Penn et al., 1998; Cang et al., 2005) into one eye, and we injected saline into the other eye of CB2-GFP:β2nAChR+/+ (WT) mice every from P4 to P10. We then examined the pattern of tOFF-αRGCs projections to the SC on P10. Since all the GFP^+ tOFF-αRGCs in each eye project to the contralateral SC (supplemental figures 2 and 4), we could directly compare the retinocollicular projections from the epi-treated retina to the retinocollicular projections from the saline-treated retina, in the two SC hemispheres of the same mouse. In the SC hemisphere contralateral to the saline-injected eye, tOFF-αRGC axons were restricted normally to the lSGS and organized into distinct columns (Figure 8A–B). In the SC hemisphere contralateral to the epi-treated eye, laminar specificity was normal but columnar specificity was perturbed (Figure 8A–B). The defects in columnar specificity induced by epi treatment were nearly as severe as those observed in CB2-GFP:β2nAChR−/− mice (Figure 8C). We therefore conclude that β2nAChR-mediated spontaneous activity that occurs in the retina from P4-P10 mediates columnar-specific refinement of tOFF-αRGC projections to the SC.

DISCUSSION

Elucidation of the map of projections from a mosaic of RGCs

We provide the first description of a complete mosaic of RGCs (tOFF-αRGCs) selectively labeled with GFP. This enabled us to relate the mosaic spacing, dendritic anatomy, and electrophysiology of these RGCs with their complete map of connections in the brain. Mouse tOFF-αRGCs are thought to be homologous to OFF-brisk-transient-Y RGCs in cats and monkeys (Pang et al., 2003; Schubert et al., 2005; Volgyi et al., 2005; Berson, 2008). However, the complete pattern of projections arising from tOFF-α/Y RGCs has not previously been elucidated. We find here that tOFF-αRGCs are remarkably specific with respect to which brain nuclei they project to, and the organization of their projections within the retinotopic maps of those nuclei. In the mouse, tOFF-αRGCs project only to the dLGN and the SC and within both these targets, they form precisely targeted laminar-specific connections. Laminar-specificity of retinocollicular projections from functionally distinct RGCs has been observed previously by recording from and filling individual RGC axons in the optic tract of cats, monkeys and hamsters (Bowling and Michael, 1980; Berson, 1988; Mooney and Rhoades, 1990; Tamamaki et al., 1995) and was suggested from retrograde filling experiments in mice (Hofbauer and Drager, 1985). Those studies agree with our

findings that α/Y RGCs project to the lSGS. But because previous studies relied on filling of randomly-targeted individual RGC axons, our results are the first to delineate the pathway corresponding to a complete mosaic of one subtype of RGCs.

Whereas laminar organization of retinogeniculate projections from functionally distinct RGCs is a hallmark feature of the carnivore and primate visual pathway (Callaway, 2005), this feature was thought to be absent in rodents (Reese, 1988). We find, however, that tOFF-αRGCs project to stereotyped lamina in the dLGN of the mouse, revealing an unexpectedly high degree of synaptic specificity in the rodent visual system. Our discovery that the axons from the mosaic of tOFF-αRGCs form a columnar map in the SC reveals the precision with which single RGC subtypes arrange their projections within a topographic map. These results and those in recent reports (Yonehara et al., 2008; Kim et al., 2008) highlight the usefulness of genetic methods to identify functionally distinct RGC subtypes and to delineate their projections within multiple brain targets, even when those targets consist of compact neuropil with no obvious cytoarchitectural divisions.

Emergence of synaptic specificity in the mammalian CNS involves axonal refinement

Our results show that mammalian RGC projections achieve laminar and columnar specificity by first transitioning through a period of imprecision (Figure 4). The emergence of synaptic specificity in the mammalian visual system thus differs from that of the invertebrate CNS where laminar and columnar specificity of photoreceptor projections emerge by directed growth of appropriately targeted synaptic connections (Meinertzhagen and Hanson, 1993; Clandinin and Zipursky, 2002). It is unlikely that the imprecision we observed simply reflects tOFF-αRGCs axons contacting the proper target SC cells that have not yet migrated to their final positions, because cell migration and lamination in the SC is completed by P5 (Edwards et al., 1986). Also, the SC follows an inside-out gradient of neurogenesis (Edwards et al., 1986), meaning that lSGS neurons develop before the uSGS. Therefore, tOFF-αRGCs project through and beyond their correct target lamina before retracting to form laminar-specific connections in the lSGS.

Spontaneous retinal activity segregates axons arising from RGCs of the same subtype

Cholinergic retinal waves are thought to segregate RGC axons from the two eyes and glutamatergic waves are thought to segregate axons from RGCs serving different functions (Torborg and Feller, 2005; Kerschensteiner and Wong, 2008). Here we provide evidence that cholinergic spontaneous retinal activity also segregates axons arising from RGCs in the same eye and of the same subtype. In previous studies, the consequences of altering spontaneous activity were assessed either by, i) randomly labeling individual RGC axons (Sretavan et al., 1988), ii) labeling all the RGC axons arising each eye (Penn et al., 1998; Huberman et al., 2002; Torborg and Feller, 2005) or iii) by labeling groups (~500) of axons arising from retinotopically-close but functionally-diverse RGCs (Grubb et al., 2003; McLaughlin et al., 2003; Chandrasekaran et al., 2005). Thus, it was unclear precisely which features of axon targeting and refinement were impacted by activity. Indeed, some studies have argued that activity is merely permissive for axon growth and targeting (Crowley and Katz, 2000; Huberman et al., 2003). Our observation that retinocollicular projections are similar between β2nAChR−/− mice and control mice before refinement on P4 (Figure 5) and that laminar

specificity emerges despite manipulations that severely perturb columnar specificity (Figures 6–8) argues against a merely permissive influence of spontaneous retinal activity on axon growth. The data presented here thus identify cholinergic retinal waves as a key influence on the emergence of synaptic specificity by clustering groups of axons arising from RGCs of the same subtype.

Our finding that cholinergic spontaneous retinal activity is not necessary to refine tOFF-αRGCs projections into specific lamina within their targets differs from eye-specific laminar refinement, which clearly requires cholinergic transmission (Penn et al., 1998; Rossi et al., 2001; Muir-Robinson et al., 2002; Huberman et al., 2002; Torborg and Feller, 2005). It is worth noting that glutamatergic waves appear in β2nAChR−/− mice by P8 (Bansal et al., 2000) whereas we evaluated laminar specificity on P10 because it is the earliest age when laminar and columnar refinement are adult-like. It is therefore possible that glutamatergic waves rescue laminar specificity of tOFF-αRGC projections between P8-P10. Nevertheless, allowing an extended period of survival past P10 does not rescue columnar-specificity (Figure 6), indicating a lasting, critical role for cholinergic spontaneous retinal activity in columnar but not laminar refinement.

The fact that laminar specificity can emerge in the absence of cholinergic retinal activity is consistent with previous studies on the role of activity in lamina-specific targeting of retinal projections in the fly and chick (Inoue et al., 1997; Hiesenger et al., 2006). We also observed normal laminar-specific targeting of tOFF-αRGCs dendrites to the OFF sublamina of the IPL of CB2-GFP:β2nAChR−/− mice (data not shown), which was expected based on previous results (Bansal et al., 2000). Although we do not rule out the possibility that non-cholinergic forms of retinal spontaneous activity could mediate laminar-specific targeting of tOFF-αRGC axons or dendrites, we speculate that RGCs select their laminar-specific connections primarily on the basis of cell-type specific expression of adhesion molecules, as is the case in the fly and chick visual system (Inoue et al., 1998; Clandinin and Zipursky, 2002; Chen and Clandinin, 2008; Nern et al., 2008; Yamagata et al., 2008). In CB2-GFP mice, tOFF-αRGCs can be identified by virtue of their GFP expression early in development (supplemental figure 5) making these mice potentially useful for studying development of RGC morphology, mosaic spacing and tiling as well as for identifying candidate genes that control lamina-specific targeting of tOFF-αRGC axons and dendrites.

Activity-dependent segregation of tOFF-αRGC projections into columns: relevance to models of ocular dominance column development.

Our findings that emergence of columnar-specific projections from tOFF-αRGCs involves axonal refinement and requires spontaneous retinal activity are consistent with the classic model of cortical ocular dominance column (ODC) formation (LeVay et al., 1978; Stryker and Harris, 1986; Huberman et al., 2006) and with experiments on ODCs in the tecta of three-eyed frogs (Reh and Constantine-Paton, 1985). Our results contrast, however, with the fly visual system, where columnar targeting of photoreceptor axons is precise from the outset and does not require synaptic transmission (Hiesenger et al., 2006). This raises the question of whether, in mammals, the segregation of visual projections into columns reflects generic mechanisms of activity-dependent axon sorting that occur during development

(Adams and Horton, 2003) or whether columns serve a particular function related to the types of neural information they carry.

Along these lines, we considered what aspects of retinocollicular circuitry tOFF-αRGC columns might correspond to and why they require cholinergic spontaneous retinal activity in order to develop. Based on the mapping of retinal coordinates onto the SC in the mouse (Drager and Hubel, 1976), we determined that the size of each GFP^+ column in the SC corresponds to about 240 to 300 μm across the retina. Cholinergic waves correlate the firing of RGCs whose cell bodies are located within 0 to 300 μm of each other (McLaughlin et al., 2003). Given the average spacing of tOFF-αRGCs, cholinergic waves should correlate nearby groups of 3 to 4 GFP^+ RGCs. These measurements support the idea that the columns described here arise from the axon terminals of neighboring GFP^+ RGCs that experience correlated activity in the retina. In this way, the columns we describe can be thought of as anchoring axons arising from closely positioned RGCs of the same subtype, through Hebbian mechanisms.

Why does columnar specificity fail to develop in β2nAChR−/− mice? In these mutants, correlated RGC firing is significantly lower than normal for RGCs situated up to 300μm apart (McLaughlin et al., 2003). This should reduce Hebbian strengthening of axonal inputs from groups of GFP^+ RGCs that project to the same SC cells, and prevent weakening and elimination of RGC axons misprojecting to intercolumn zones or to incorrect columns. This model is consistent with our observation that qualitatively and quantitatively, some columnar architecture is present in both WT and β2nAChR−/− mice on P4/5 (Figure 5) and that columnar specificity is severely reduced but not entirely absent in P10 and adult β2nAChR−/− mice (Figure 6). This model is also consistent with studies that perturbed retinal waves or blocked NMDA receptors in the SC during development and observed increased receptive field sizes of SC neurons (Chandrasekaran et al., 2005; Huang and Pallas, 2001).

One consideration is that mouse tOFF-αRGCs are coupled to one another through connexin36 gap junctions (Schubert et al., 2005). Genetic removal of connexin36 abolishes tOFF-αRGC coupling (Schubert et al., 2005) and yet the same manipulation does not perturb early spontaneous retinal activity or eye-specific refinement in the dLGN (Torborg and Feller, 2005). Thus it is unlikely that genetic removal of β2nAChRs or epibatidine prevents columnar segregation of tOFF-αRGC axons by reducing gap junction coupling of these RGCs. We thus conclude that altered correlated RGC firing (Bansal et al., 2000; McLaughlin et al., 2003; Cang et al., 2005; Torborg and Feller, 2005) is the factor primarily responsible for the defective columnar refinement of tOFF-αRGC projections in CB2-GFP:β2nAChR−/− and epibatidine-treated mice.

At this time, we do not know what the columns arising from tOFF-αRGCs contribute to visual processing or behavior. Interestingly, others have described columns of somatosensory input to the deeper non-retinorecipient SC layers that are in register with the retinotopic map (Dräger and Hubel, 1976). Whether somatosensory columns align with tOFF-αRGC columns is unclear, but it is tempting to speculate about their possible relationship in multi-modal sensory integration. Ultimately, tools that allow manipulation of neural activity in particular RGC subtypes will allow us to determine their contribution

to visual perception and behavior. In the meantime, our findings show that transgenic mice with genetically identified subtypes of retinal neurons expressing GFP can serve as useful tools for elucidating previously uncharted structure-function relationships in the visual system and for studying the mechanisms underlying development of synaptic specificity in the mammalian CNS.

EXPERIMENTAL PROTOCOLS

CB2-GFP mice

Mice were obtained from the Mouse Regional Resource Center (detailed information about CB2-GFP mice, also called Calb2 or calretinin-EGFP, is available at: http://www.mmrrc.org/strains/283/0283.html). Mice were generated on Swiss-webster background and were crossed onto C57/Bl6 background for multiple generations in our laboratory. In the text, postnatal day 0 corresponds to the day of birth. GFP expression in the retina of CB2-GFP was reflective of mRNA in situ for calretinin in the retina but there was less GFP in the brain than would be expected on the basis of calretinin mRNA expression (data not shown). This reflects positional effects of the CB2-GFP transgene insertion (Gong et al., 2003).

CB2-GFP:β2nAChR−/− mice

These mice were generated by breeding β2nAChR−/− mice (Xu et al., 1999; obtained from D. Feldheim, UC Santa Cruz) to CB2-GFP mice. The CB2-GFP:β2nAChR+/− offspring were backcrossed to β2nAChR−/− mice on a C57/Bl6 background and the mixed background CB2-GFP:β2nAChR−/− offspring were then used to breed and expand the line. Genotyping was carried out as previously described (Xu et al., 1999).

Retinal histology

Mice were perfused with saline followed by 4% parformaldehyde (PFA), the eyes removed and postfixed 4 hours in 4% PFA at 4C, then the retina was extracted. For whole mount, relieving cuts made to allow the retina to lay flat. Retinas were incubated in blocking solution (10% goat serum, 0.25% Triton-X in PBS) for 2 hours, then transferred to primary antibodies (1:1000 rabbit anti-GFP from Molecular Probes; 1:5000 mouse SMI-32, Sternberger monoclonals) for 48 hours at 4C, washed in PBS (5 X 1hour), transferred to secondary antibody (1:1000 goat anti-rabbit Alexa 488, 1:1000 goat anti-mouse Alexa 594; Molecular probes) for 2 hours, washed in PBS (5 X 1hour), mounted and coverslipped with Vectashield (Vectorlabs). Retinal sections: the retina was immersed in 30% sucrose, then cryosectioned at 12μm. Block=1 hour, primary incubation=24 hours at 4C, secondary incubation=1 hour. VAChT staining (1:1000 goat anti-VAChT, Chemicon), required the use of donkey serum rather than goat serum.

DiI labeling of single RGCs

Methods were as described previously (Kim and Jeon, 2006). Whole eyes were fixed for 8 hours in 4% PFA, the retina extracted and stored in PBS. GFP^+ cells were filled iontophoretically using an Axoprobe-1A amplifier and the lipophilic dye, DiI. Electrodes had resistances of about 50 MOhm and were about 0.5μm in size. A positive current of between 5 and 20nA was applied for 20–30 minutes to fill each cell.

Quantification of GFP$^+$ RGCs

The number of GFP$^+$ RGCs per retina was counted from 5X or 10X montaged images of whole mount stained retinas. t-tests were applied for statistical comparisons here and unless otherwise noted, for all quantitative measurements listed below. SEMs are shown.

Quantification of mosaic regularity

The density recovery profile (Rodieck, 1991) describes the average density of cells at a given distance from the soma, and was calculated as

$$\rho(s) = \frac{\sum_i n_i(s)}{\sum_i A_i(s)} \quad (1)$$

where $n_i(s)$ is a histogram of the number of cells in an image at distance s from cell i, and $A_i(s)$ is the area contained in that image at distance s from cell i. $\rho(s)$ was calculated from all GFP$^+$ RGCs in 27 images of central and peripheral retina from 6 different mfice.

Electrophysiology

The dark-adapted mouse retina was isolated under an infrared microscope into oxygenated Ringer's solution (124 mM NaCl, 2.5 mM KCl, 2 mM $CaCl_2$, 2 mM $MgCl_2$, 1.25 mM NaH_2PO_4, 26 mM $NaHCO_2$ and 22.2 mM glucose) and the pH was maintained at 7.4 pH by bubbling of 95% O_2, 5% CO_2 at 36 °C. A flattened retina-eyecup preparation (Hu et al., 2000) was placed with ganglion cells facing upwards in a superfusion chamber on the stage of an upright fluorescence microscope and held in place with a transparent dialysis membrane containing several ~200 μm holes. For intracellular recordings, sharp microelectrodes were filled with 2 M potassium acetate, having a final impedance of 250–350 MΩ. Fluorescent retinal ganglion cells were detected at x40 magnification by excitation with a blue LED. To minimize effects of adaptation and photodamage, single fluorescent images were taken at a very dim excitation intensity (~10 mW/m^2), within the range of intensities used for visual stimulation, and exposed for 10–20 s. To facilitate direct access to the ganglion cell soma by the intracellular electrode, the inner limiting membrane was microdissected using a patch pipette. After a fluorescent cell was identified, it was impaled under oblique infrared illumination.

Stimulation and analysis: Light stimuli were projected from a computer video monitor through a custom-made lens system and focused from above onto the photoreceptor layer through a x10 water immersion objective a mean photopic intensity of ~8 mW/m^2. Flashes (0.5 Hz) were presented using the maximum and minimum intensities of the monitor. The spatio-temporal receptive field of all neurons was measured by the standard method of reverse-correlation of the membrane potential to a flickering checkerboard stimulus (110 μm regions changing every 30 ms) (Baccus et al, 2008).

To compute correlation coefficients between the average flash responses of neurons, spikes were first removed by setting a threshold for the derivative of the membrane potential, and then the average was computed from 10 – 15 flashes. The correlation coefficient r between two average flash responses $x(t)$ and $y(t)$ was calculated as

$$r = \frac{\int_0^T (x(t) - \langle x \rangle)(y(t) - \langle y \rangle)dt}{\sqrt{\int_0^T (x(t) - \langle x \rangle)^2 dt}\sqrt{\int_0^T (y(t) - \langle y \rangle)^2 dt}} \quad (2)$$

where T is the duration of the recording, and $\langle \ldots \rangle$ denotes the time average.

Brain histology

Mice were perfused, brains removed, postfixed for 8 hours in 4% PFA, immersed in 30% sucrose, and sectioned at 30μm on a freezing microtome. GFP staining was carried out as above except that primary antibody incubation was overnight at 4C and secondary incubation was 90min at RT. CTb-594 was visualized without immunostaining.

CTb-594 labeling of RGC axons

2–5μl of CTb-594 (0.5% diluted in saline; Molecular Probes) was injected into the vitreous of each eye (2μl/eye on P4/5, 3.5μl/eye at P10; 5μl/eye in adults). The mouse was perfused 24 hours later (ages in text refer to age of animal at perfusion). CTb-594 was visualized without any immunostaining.

Epibatidine treatment

1μl of 1mM epi was injected into the vitreous of one eye every 48 hours on P4, P6, P8 (Rossi et al., 2001). An equivalent volume of saline vehicle was injected into the opposite eye and both eyes were labeled with CTb-594 on P9, and brain tissue harvested on P10.

Quantification of retinorecipient SC depth

The distance from the base of the SO to the pial surface of the SC was measured from CTb-594 labeling at four locations across each SC section. Measures were taken from 2–4 SC sections per animal, and averaged before statistical comparison.

Quantification of laminar specificity

The depth of the retinorecipient SC was divided into quarters along its depth such that the pial margin was 0% and the base of the SO was 100%. 0–50% depth corresponds well to the combined thickness of the uSGS and SZ. 1.5–2mm line scans were made across the rostral-caudal (sagittal sections) and medial lateral (coronal sections) SC and the number of GFP^+ axons intersected per mm was calculated in the 0–25% and 25–50% depths. 2–4 sections per animal were analyzed to generate an average per animal. The density of GFP labeling in the 50–75% and 75–100% depths of the SC (the lSGS and SO) was too high to count individual axons. We therefore quantified the degree of mistargeting to the 0–50% depth (the uSGS and SZ).

Quantification of columnar specificity

To measure the degree of columnar specificity in the SC, we calculated a column segregation index (*CSI*) (Crowley and Katz, 2000) according to

$$CSI = 1 - \frac{m - b}{c - b} \quad (3)$$

where c is the image intensity in the center of a fluorescent patch, m is the intensity at the midpoint between patches, and b is the intensity of the background tissue, measured in square regions 100 μm on a side. CSI ranged between 0 and 1, and was averaged over all adjacent patch/interpatch pairs in 2–4 SC sections per animal. Sample sizes reflect the number of animals. For no age or condition was the CSI zero, indicating that some columnar structure was present even on P4 and after activity manipulations. The near-complete lack of columnar segregation in some CB2-GFP:β2nAChR−/− mice made it difficult to identify interpatch zones in those animals. We therefore made line scans across the extent of the lSGS and took the troughs as interpatch zones.

Supplementary Material

Refer to Web version on PubMed Central for supplementary material.

ACKNOWLEDGEMENTS

We are grateful to D. Feldheim, T. Clandinin, T. Cutforth and J. Krey for helpful comments and suggestions. We thank B. Chapman for use of her microscope and J. Yamada and M. Martin for genotyping. This work was supported by NIH RO1 NIH R21 EY018320 (B.A.B), NIH R01 EY016842 (S.B). A March of Dimes Basil O'Connor Award (E. M. U), Research to Prevent Blindness Young Investigator Award (E.M.U.), NIH EY02162 (E.M.U.), and NIH R21MH083090 (E.M.U.) and T32 EY07120 (S.K.). A. Huberman was supported by a Helen Hay Whitney Postdoctoral Fellowship.

REFERENCES

Adams DL, and Horton JC (2003). Capricious expression of cortical columns in the primate brain. Nat Neurosci. 6, 113–4. [PubMed: 12536211]

Baccus SA, Olveczky BO, Manu M, and Meister M (2008). A retinal circuit that computes object motion. J. Neurosci 28, 6807–6817. [PubMed: 18596156]

Bansal A, Singer JH, Hwang BJ, Xu W, Beaudet A, and Feller MB (2000). Mice lacking specific nicotinic acetylcholine receptor subunits exhibit dramatically altered spontaneous activity patterns and reveal a limited role for retinal waves in forming ON and OFF circuits in the inner retina. J. Neurosci 20, 7672–81. [PubMed: 11027228]

Benson DL, Colman DR, and Huntley GW (2001). Molecules, maps and synaptic specificity. Nat. Rev. Neurosci 2, 899–909. [PubMed: 11733797]

Berson DM (1988). Retinal and cortical inputs to cat superior colliculus: composition, convergence and laminar specificity. Prog. Brain Res 75, 17–26. [PubMed: 3055056]

Berson DM (2008). Retinal ganglion cell types and their central projections. In: The Senses: A Comprehensive Reference. Vol 1, pp. 491–520. San Diego, Academic press.

Bowling DB, and Michael CR (1980). Projection patterns of single physiologically characterized optic fibres in cat. Nature 286, 899–902. [PubMed: 7412871]

Callaway EM (2005). Structure and function of parallel pathways in the primate early visual system. J. Physiol 566, 13–9. [PubMed: 15905213]

Cang J, Renteria RC, Kaneko M, Liu X, Copenhagen DR, and Stryker MP (2005). Development of precise maps in visual cortex requires patterned spontaneous activity in the retina. Neuron 48, 797–809. [PubMed: 16337917]

Chandrasekaran AR, Plas DT, Gonzalez E, and Crair MC (2005). Evidence for an instructive role of retinal activity in retinotopic map refinement in the superior colliculus of the mouse. J. Neurosci 25, 6929–38. [PubMed: 16033903]

Chen PL, and Clandinin TR (2008). The cadherin Flamingo mediates level-dependent interactions that guide photoreceptor target choice in Drosophila. Neuron 58, 26–33. [PubMed: 18400160]

Clandinin TR, and Zipursky SL (2002). Making connections in the fly visual system. Neuron 35, 827–41. [PubMed: 12372279]

Crowley JC, and Katz LC (2000). Early development of ocular dominance columns. Science 290, 1321–4. [PubMed: 11082053]

Demas J, Eglen SJ, and Wong RO (1993). Developmental loss of synchronous activity in the mouse retina is independent of visual experience. J. Neurosci 25, 9347–57.

Edwards MA, Caviness VS, and Schneider GE (1986). Development of cell and fiber lamination in the mouse superior colliculus. J. Comp. Neurol 248, 395–409. [PubMed: 3722463]

Famiglietti EV, and Kolb H (1976). Structural basis for ON- and OFF-center responses in retinal ganglion cells. Science 194, 193–5. [PubMed: 959847]

Farah MH, and Easter SS (2005). Cell birth and death in the mouse retinal ganglion cell layer. J. Comp. Neurol 289, 120–34.

Gong S, Zheng C, Doughty ML, Losos K, Didkovsky N, Schambra UB, Nowak NJ, Joyner A, Leblanc G, Hatten ME, and Heintz N (2003). A gene atlas of the central nervous system based on bacterial artificial chromosomes. Nature 425, 917–25. [PubMed: 14586460]

Grubb MS, Rossi FM, Changuex JP, and Thompson ID (2003). Abnormal functional organization in the dorsal latera; geniculate nucleus of mice lacking the beta 2 subunit of the nicotinic acetylcholine receptor. Neuron 30, 1151–72.

Hiesinger PR, Zhai RG, Zhou Y, Koh TW, Mehta SQ, Schulze KL, Cao Y, Verstreken P, Clandinin TR, Fischbach KF, Meinertzhagen IA, and Bellen HJ (2006). Activity-independent prespecification of synaptic partners in the visual map of Drosophila. Curr. Biol 16, 1835–43. [PubMed: 16979562]

Hofbauer A, and Dräger UC (1985). Depth segregation of retinal ganglion cells projecting to the mouse superior colliculus. J. Comp. Neurol 234, 465–74. [PubMed: 3988995]

Hu EH, Dacheux RF, and Bloomfield SA (2000). A flattened retina-eyecup preparation suitable for electrophysiological studies of neurons visualized with transscleral infrared illumination. J Neurosci Methods 103, 209–16. [PubMed: 11084214]

Huang L, and Pallas SL (2001). NMDA antagonists in the superior colliculus prevent developmental plasticity but not visual transmission. J Neurophysiol. 86, 1179–94. [PubMed: 11535668]

Huberman AD, Stellwagen D, and Chapman B (2002). Decoupling eye-specific segregation from lamination in the lateral geniculate nucleus. J Neurosci 22, 9419–29. [PubMed: 12417667]

Huberman AD, Wang GY, Liets LC, Collins OA, Chapman B, and Chalupa LM (2003). Eye-specific segregation independent of normal neuronal activity. Science 300, 994–8. [PubMed: 12738869]

Huberman AD, Speer CM, and Chapman B (2006). Spontaneous retinal activity mediates development of ocular dominance columns and binocular receptive fields in v1. Neuron 52, 247–54. [PubMed: 17046688]

Inoue A, and Sanes JR (1997). Lamina-specific connectivity in the brain : regulation by N-cadherin, neurotrophins, and glycoconjugates. Science 276, 1428–31. [PubMed: 9162013]

Kim TJ, and Jeon CJ (2006). Morphological classification of parvalbumin-containing retinal ganglion cells in mouse: single cell injection after immunocytochemistry. Invest. Ophthalmol. Visual Sci 47, 2757–64. [PubMed: 16799011]

Kim IJ, Zhang Y, Yamagata M, Meister M, and Sanes JR (2008). Molecular identification of a retinal cell type that responds to upward motion. Nature 452, 478–82. [PubMed: 18368118]

Kerschensteiner D, and Wong RO (2008). A precisely timed asynchronous pattern of ON and OFF retinal ganglion cell activity during propagation of retinal waves. Neuron 58, 851–8. [PubMed: 18579076]

Kong JH, Fish DR, Rockhill RL, and Masland RH (2005). Diversity of ganglion cells in the mouse retina: unsupervised morphological classification and its limits. J. Comp. Neurol 489, 293–310. [PubMed: 16025455]

Lee EJ, Kim HJ, Lim EJ, Kim IB, Kang WS, Oh SJ, Rickman DW, Chung JW, and Chun MH (2004). AII amacrine cells in the mammalian retina show disabled-1 immunoreactivity. J. Comp. Neurol 470, 372–81. [PubMed: 14961563]

LeVay S, Stryker MP, and Shatz CJ (1978). Ocular dominance columns and their development in layer IV of the cat's visual cortex: a quantitative study. J Comp Neurol 179, 223–44. [PubMed: 8980725]

Luo L, and Flanagan JG (2007). Development of continuous and discrete neural maps. Neuron 56, 284–300. [PubMed: 17964246]

May PJ (2005). The mammalian superior colliculus: laminar structure and connections. Prog. Brain Res 151, 321–78.

McLaughlin T, Torborg CL, Feller MB, and O'Leary DD (2003). Retinotopic map refinement requires spontaneous retinal waves during a brief critical period of development. Neuron 40, 1147–60. [PubMed: 14687549]

McLaughlin T, and O'Leary DD (2005). Molecular gradients and development of reitnotopic maps. Annu. Rev. Neurosci 28, 327–55. [PubMed: 16022599]

Meinertzhagen IA, and Hansen TE (1993). The development of the optic lobe. In: The Development of Drosophila Melanogaster, CSHL Press, NY. pp 1363–1491.

Mooney RD, and Rhoades RW (1990). Relationships between physiological and morphological propoeties of retinocollicular axons in the hamster. J. Neurosci 10, 3164–77. [PubMed: 2398377]

Nern A, Zhu Y, and Zipursky SL (2008). Local N-cadherin interactions mediate distinct steps in the targeting of lamina neurons. Neuron 58, 34–41. [PubMed: 18400161]

Pang JJ, Gao F, and Wu SM (2003). Light-evoked excitatory and inhibitory synaptic inputs to ON and OFF alpha ganglion cells in the mouse. J. Neurosci 23, 6063–73. [PubMed: 12853425]

Peichl L (1991). Alpha ganglion cells in mammalian retinae: common properties, species differences, and some comments on other ganglion cells. Visual Neurosci. 7, 155–69.

Penn AA, Riquelme PA, Feller MB, and Shatz CJ (1998). Competition in retinogeniculate patterning driven by spontaneous activity. Science 279, 2108–12. [PubMed: 9516112]

Picciotto MR, Zoli M, Lena C, Bessis A, Lallemand Y, Le Novere N, Vincent P, Pich EM, Brulet P, and Changuex JP (1995). Abnormal avoidance learning in mice lacking functional high-affinity nicotinic in the brain. Nature 374, 65–7. [PubMed: 7870173]

Reese BE (1988). 'Hidden lamination in the dorsal lateral geniculate nucleus: the functional organization of this thalamic region in the rat. Brain Res. 472, 119–37. [PubMed: 3289687]

Reh TA, and Constantine-Paton M (1985). Eye-specific segregation requires neural activity in three-eyed Rana pipiens. J. Neurosci 5, 1132–43. [PubMed: 3873522]

Renteria RC, Tian N, Cang J, Nakanishi S, Stryker MP, and Copenhagen DR (2006). Intrinsic On responses of the retinal OFF pathway are suppressed by the ON pathway. J. Neurosci 26, 11857–69. [PubMed: 17108159]

Rodieck RW (1991). The density recovery profile: a method for the analysis of points in the plane applicable to retinal studies. Vis. Neurosci 6, 95–111. [PubMed: 2049333]

Roska B, Werblin F (2001). Vertical interactions across ten parallel, stacked representations in the mammalian retina. Nature 410, 583–7. [PubMed: 11279496]

Rossi FM, Pizzorusso T, Porciatti V, Marubio LM, Maffei L, Changuex JP (2001). Requirement of the nicotinic acetylcholine receptor b2 subunit for the anatomical and functional development of the visual system. Proc Natl Acad USA 98, 6453–6458.

Sachs GM, Jacobson M, and Caviness VS (1986). Postnatal changes in arborization patterns of murine retinocollicular axons. J. Comp. Neurol 246, 395–408. [PubMed: 3700722]

Schubert T, Degen J, Willecke K, Hormuzdi SG, Monyer H, and Weiler R (2005). Connexin36 mediates gap junctional coupling of alpha-ganglion cells in mouse retina. J. Comp. Neurol 485, 191–201. [PubMed: 15791644]

Sretavan DW, Shatz CJ, and Stryker MP (1988). Modification of reitnal ganglion cell axon morphology by prenatal infusion with tetrodotoxin. Nature 336, 468–71. [PubMed: 2461517]

Stryker MP, and Harris WA (1986). Binocular impulse blockade prevents the formation of ocular dominance columns in cat visual cortex. J Neurosci. 6, 2117–33. [PubMed: 3746403]

Sun W, Li N, and He S (2002). Large-scale morphological survey of mouse retinal ganglion cells. J. Comp. Neurol 451, 115–26. [PubMed: 12209831]

Tamamaki N, Uhlrich DJ, and Sherman SM (1995). Morphology of physiologically identified retinal X and Y axons in the cat's thalamus and midbrain as revealed by intraaxonal injection of biocytin. J. Comp. Neurol 354, 583–607. [PubMed: 7608339]

Torborg CL, and Feller MB (2005). Spontaneous patterned retinal activity and the refinement of retinal projections. Prog. Neurobiol 76, 213–35. [PubMed: 16280194]

Volgyi B, Abrams J, Paul DL, and Bloomfield SA (2005). Morphology and tracer coupling pattern of alpha ganglion cells in the mouse retina. J. Comp. Neurol 492, 66–77. [PubMed: 16175559]

Wässle H (2004). Parallel processing in the mammalian retina. Nat. Rev. Neurosci 5, 747–57. [PubMed: 15378035]

Wong RO (1999). Retinal waves visual system development. Annu. Rev. Neurosci 22, 29–47. [PubMed: 10202531]

Xu W, Orr-Utreger A, Nigro F, Gelber S, Sutcliffe CB, Armstrong D, Patrick JW, Role LW, Beaudet AL, and De Biasi M (1999). Multiorgan autonomic dysfunction in mice lacking the beta2 and the beta4 subunits of neuronal nicotinic acetylcholine receptors. J Neurosci. 19, 9298–305. [PubMed: 10531434]

Yamagata M, and Sanes JR (2008). Dscam and Sidekick proteins direct lamina-specific synaptic connections in vertebrate retina. Nature 451, 465–9. [PubMed: 18216854]

Yonehara K, Shintani T, Suzuki R, Sakuta H, Takeuchi Y, Nakamura-Yonehara K, and Noda M (2008). Expression of SPIG1 reveals development of a retinal ganglion cell subtype projecting to the medial terminal nucleus in the mouse. PloS ONE. 3, e1533. [PubMed: 18253481]

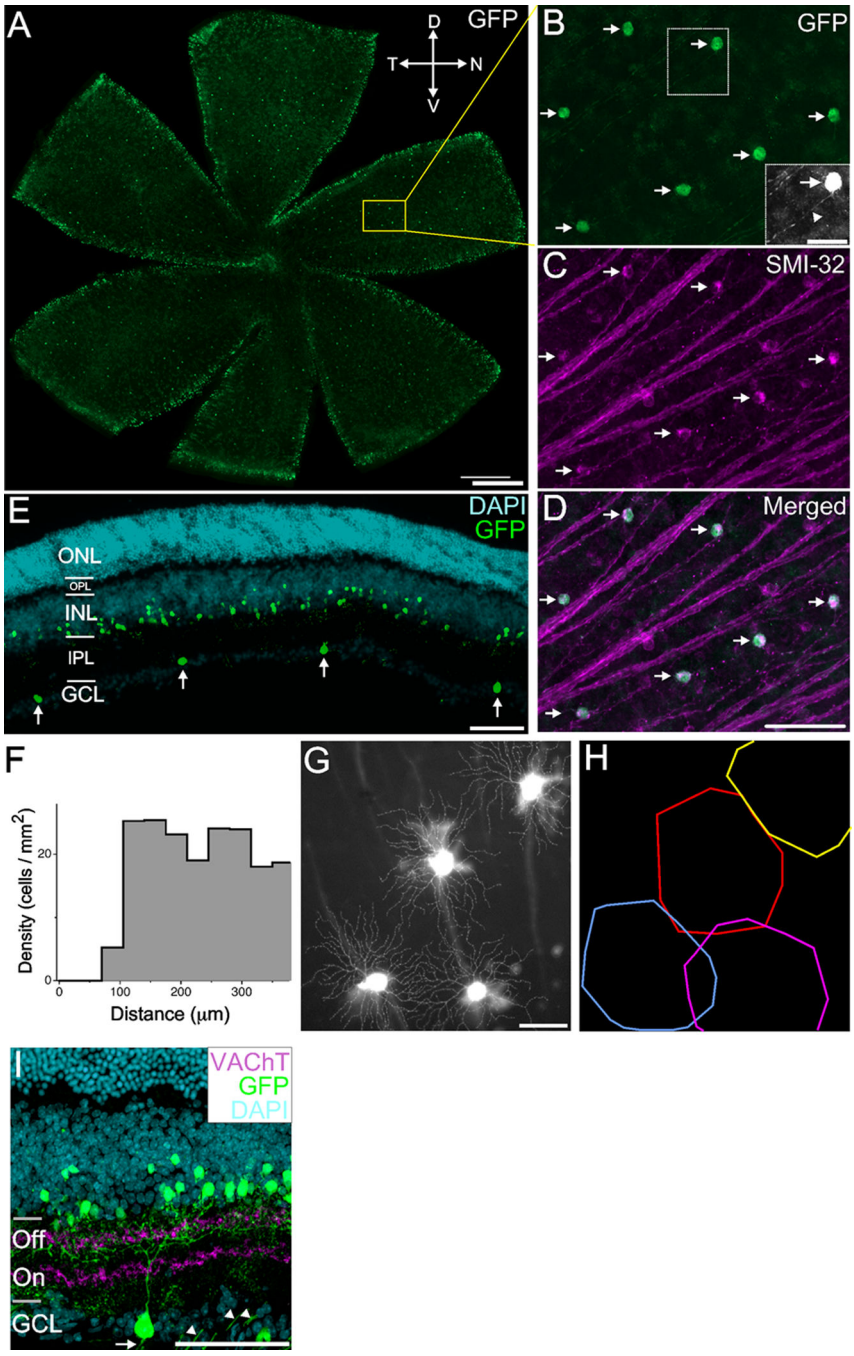

Figure 1. A mosaic of GFP$^+$ OFF-αRGCs in CB2-GFP mice.

(A) Whole-mount CB2-GFP retina, showing GFP$^+$ RGCs. Along the relieving cuts, GFP$^+$ amacrine cells are also evident (see E). D/V/N/T: dorsal, ventral, nasal, temporal axes. Scale is 500 μm. (B-D) High magnification of the boxed region in (A). (B) GFP$^+$ RGCs (arrows). Inset shows a single GFP$^+$ RGC (arrow) with its axon (arrowhead). (C, D) Every GFP$^+$ RGC is immunopositive for SMI-32 (SMI-32$^+$). Scale in B-D is 125 μm. Scale in B inset is 50 μm. (E) Vertically-sectioned retina. Blue, DAPI staining indicates cellular layers. GFP$^+$ cells are amacrine cells in the inner nuclear layer (INL), and regularly spaced RGCs in the

GCL (arrows). Scale is 100 μm. (F) Density profile of GFP^+ RGC cells as a function of distance from other GFP^+ RGCs (Rodieck, 1991). (G) Four neighboring GFP^+ RGCs filled with DiI to reveal their entire dendritic arbors. (H) Dendritic field boundaries of the same four GFP^+ cells. (G, H) Scale is 75 μm. (I) Retinal section stained for DAPI, GFP and the vesicle-acetylcholine transporter (VAChT) which labels the middle of the ON and OFF sublaminae in the IPL (horizontal lines denote boundaries of IPL). GFP^+ RGC dendrites ramify within the OFF sublaminae at the ~30–35% depth of the IPL. Arrow indicates the GFP^+ RGC's axon. Arrowheads indicate axons from other GFP^+ RGCs whose somata lie outside the field of view. Scale is 75 μm.

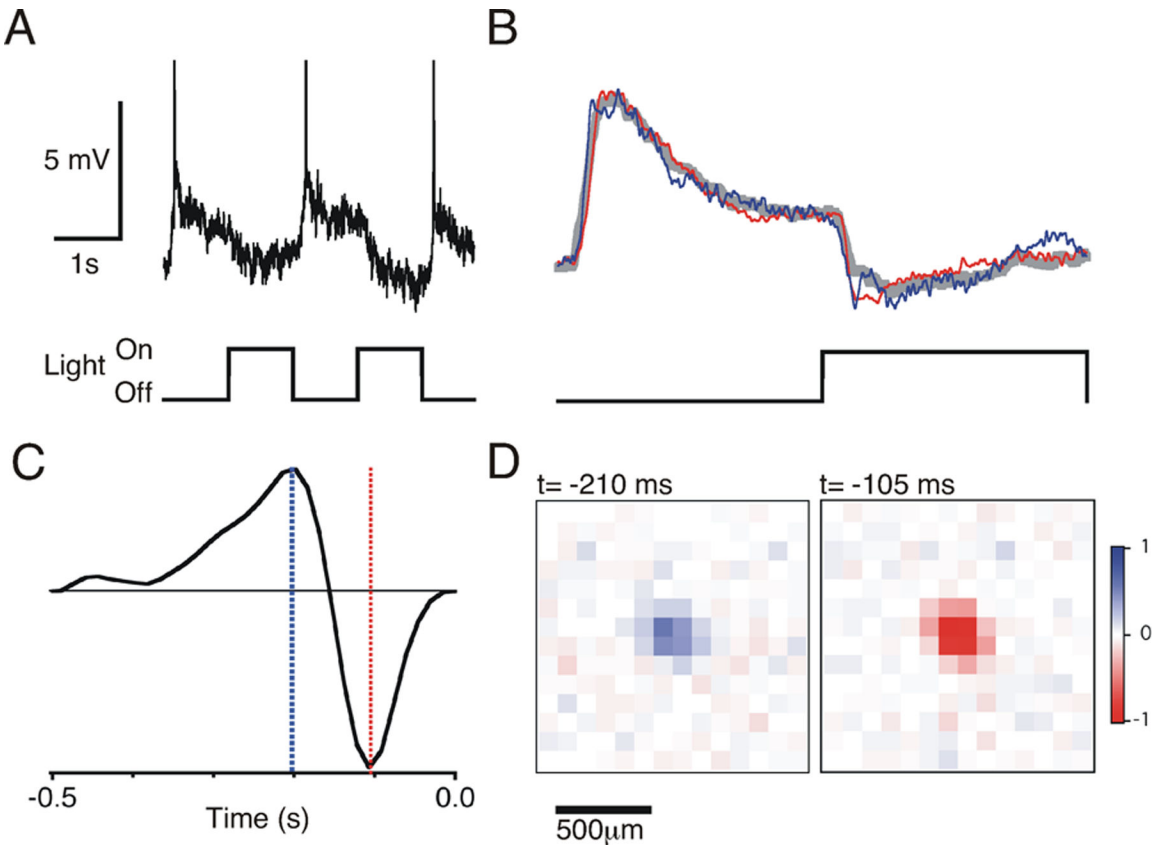

Figure 2. Visual responses of GFP$^+$ tOFF-αRGCs.

A) Membrane potential response of a GFP$^+$ tOFF-αRGC in response to a 1 s periodic flash. Action potentials are truncated. B) Average subthreshold flash response of 7 cells (gray trace), compared to the average flash response of two example cells (colored traces). Spikes were digitally removed prior to averaging. (C-D) Spatio-temporal receptive field of a GFP$^+$ tOFF-αRGC computed from the membrane potential response of the cell to a randomly flickering checkerboard. C) Temporal filter averaged across the spatial receptive field center. D) Two spatial slices of the receptive field taken at the times indicated by the colored lines in C, indicating the biphasic nature of the receptive field center.

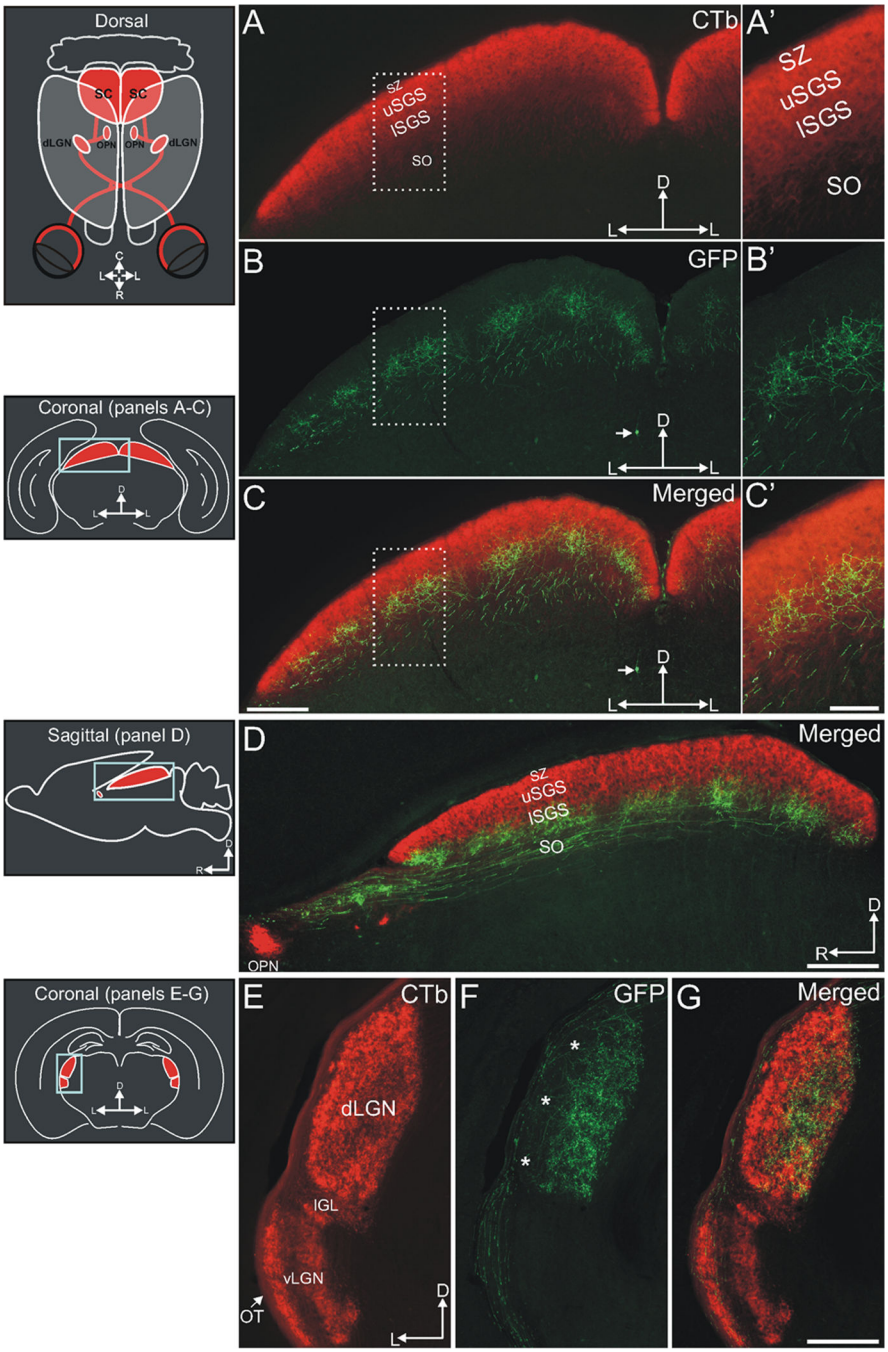

Figure 3. Axonal projections of GFP$^+$ tOFF-αRGCs.

(Left margin) Schematics of RGC projections in the mouse. (Top left) Dorsal view. The retinas and optic pathways are in red. Superior colliculus (SC), dorsal lateral geniculate nucleus (dLGN) and olivary pretectal nucleus (OPN). Here and in (A-G) R: rostral, C: caudal, L: lateral, M: medial. Schematics of coronal and sagittal view of the brain at the level of the SC (Middle panels) and dLGN (bottom panel). (A-D) Laminar- and columnar-specific tOFF-αRGC axonal projections to the SC. (A) CTb-594 labeling (red) of all RGC axons. CTb-594 weakly labels RGC axon shafts but densely labels RGC axon

terminals and thereby completely labels all retinorecipient nuclei. SO, stratum opticum; lSGS, lower stratum griseum superficialis; uSGS, upper stratum griseum superficialis; SZ, stratum zonale. (A') High magnification view of box in (A). (B) GFP^+ tOFF-αRGC axons in the SC. The axons enter the SC through the SO, and selectively arborize in the lSGS. The GFP^+ arbors are also organized into columns. Small arrow indicates a GFP^+ cell in the deeper SC; such cells do not contribute to the GFP^+ axons in the retinorecipient SC (see supplemental figure 2). (B') High magnification view of box in (B). (C) Merged view of (A) and (B). (C') High magnification view of box in (C). (A-C) Scale is 250 μm. Coronal plane is shown; D: dorsal, L: lateral. A-C. Scale in A'-C' is 125μm. (D) Sagittal view of CTb-594^+ and GFP^+ tOFF-αRGC axons in the SC. Scale is 250 μm. (E-G) Retino-dLGN projections viewed in the coronal plane. (E) CTb-594 labeled RGC axons fill the entire dLGN, IGL and vLGN. OT, optic tract. (F) GFP^+ tOFF-αRGC axons bypass the vLGN and IGL, turn medially into the dLGN and project through the lateral third of the dLGN (asterisks) to selectively arborize in the inner dLGN, forming a "layer". (G) Merged view of (E) and (F). Scale is 250 μm.

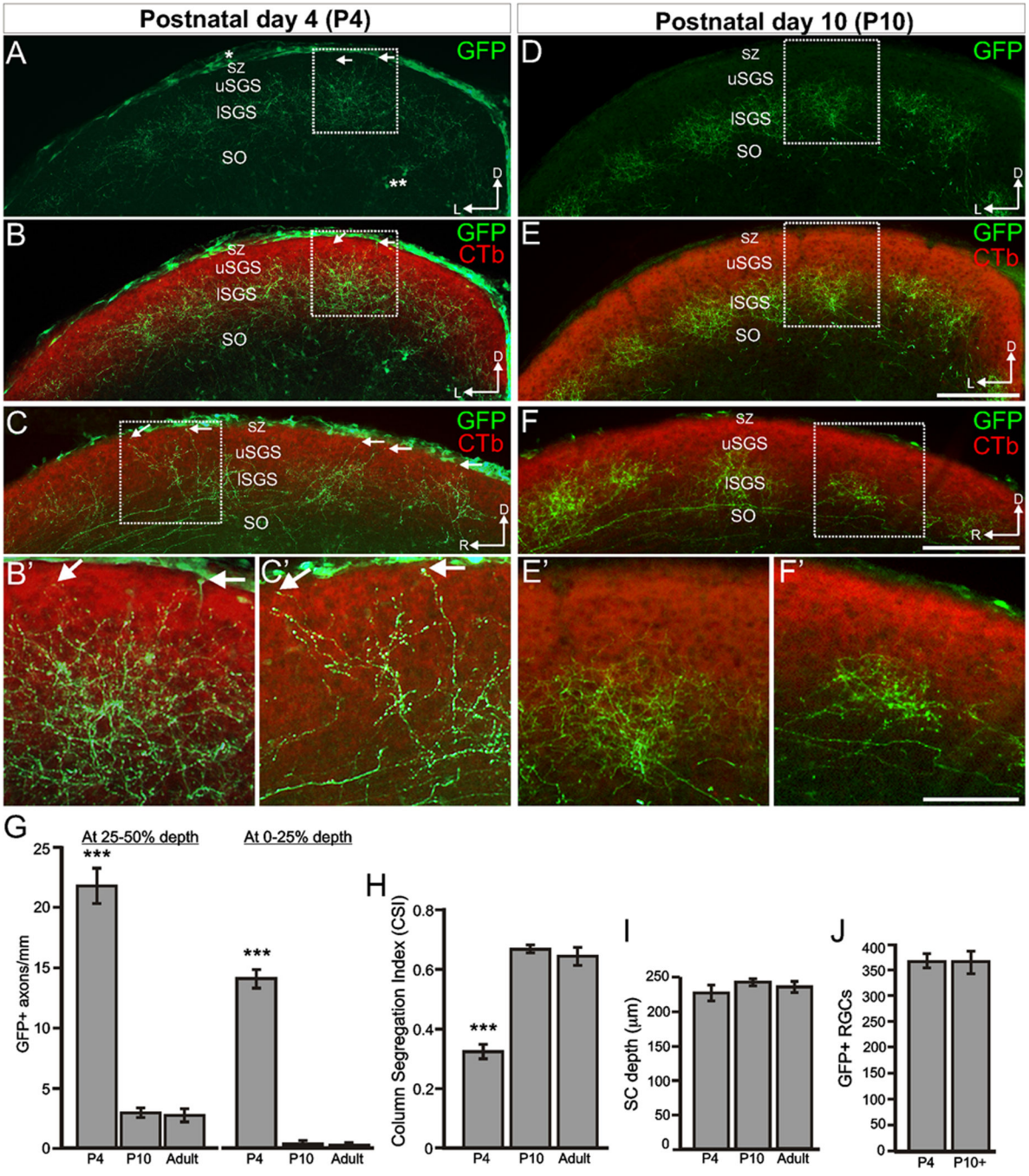

Figure 4. Development of laminar- and columnar-specific tOFF-αRGC projections involves axonal refinement.

(A-C') Targeting of tOFF-αRGC axons to the SC is imprecise early in development. (A, B) Coronal view of the SC in a P4 CB2-GFP mouse. tOFF-αRGC axons exhibit rudimentary columnar- and laminar-specificity, but unlike in adult CB2-GFP mice (Figure 3) many GFP^+ axons project into the uSGS and SZ, and up to the pial margin (arrows). (B') Higher magnification view of the boxed region in (A, B). Arrows indicate GFP^+ axons projecting to the uppermost SC. (C, C') Sagittal view of the SC on P4. GFP^+ axons are distributed across the retinorecipient depth of the SC. Arrows indicate GFP^+ axons projecting to the

pial margin (arrows). Asterisks in (A) indicate GFP^+ glia at the pial margin and a few GFP^+ neurons in the deeper, non-retinorecipient SC (see Figure 3). GFP expression in these glia disappears by ~P8. Neither the GFP^+ glia nor GFP^+ SC neurons contribute to the GFP^+ axons in the young or adult SC (supplemental figures 2 and 3). (D-F') Targeting of tOFF-αRGC axons to the SC is adult-like by P10; GFP^+ axons are restricted to the lSGS and segregated into distinct columns. (A-F) Scale is 250 μm. (B',C',E',F') Scale is 125 μm. (G) Quantification of laminar-specificity as a function of age (see experimental procedures). The number of GFP^+ axons/mm projecting to the 25–50% (upper third) and 0–25% (upper quarter) of the SC depth is significantly greater on P4 compared to P10 or adult ($p<0.0001$). P10 versus adult were not significantly different (25–50% depth, $p=0.74$; 0–25% depth, $p=0.23$; t-test, ±SEM) (n=4 adult mice, n=6 P10 mice, n=7 P4 mice). (H) Columnar segregation index (see experimental protocols). There is significantly less columnar-specificity on P4, as compared to P10 or adult ($p<0.0001$), whereas columnar-specificity is indistinguishable between P10 and adult ($p=0.53$) (n=3 mice per age). (I) The depth (retinorecipient thickness) of the SC is not different between P4, P10, or adult CB2-GFP mice (P4 vs. P10, $p=0.3$; P4 vs. adult, $p=0.48$; t-test) (n=5 P4 mice, n=4 P10 mice, n=4 adult mice). (J) The number of GFP^+ RGCs per retina is not different on P4 compared to P10 and adult (P10+) ($p=0.96$; t-test; ±SEM; n=5 P4 mice, n=4 P10 mice, and n=4 adult mice).

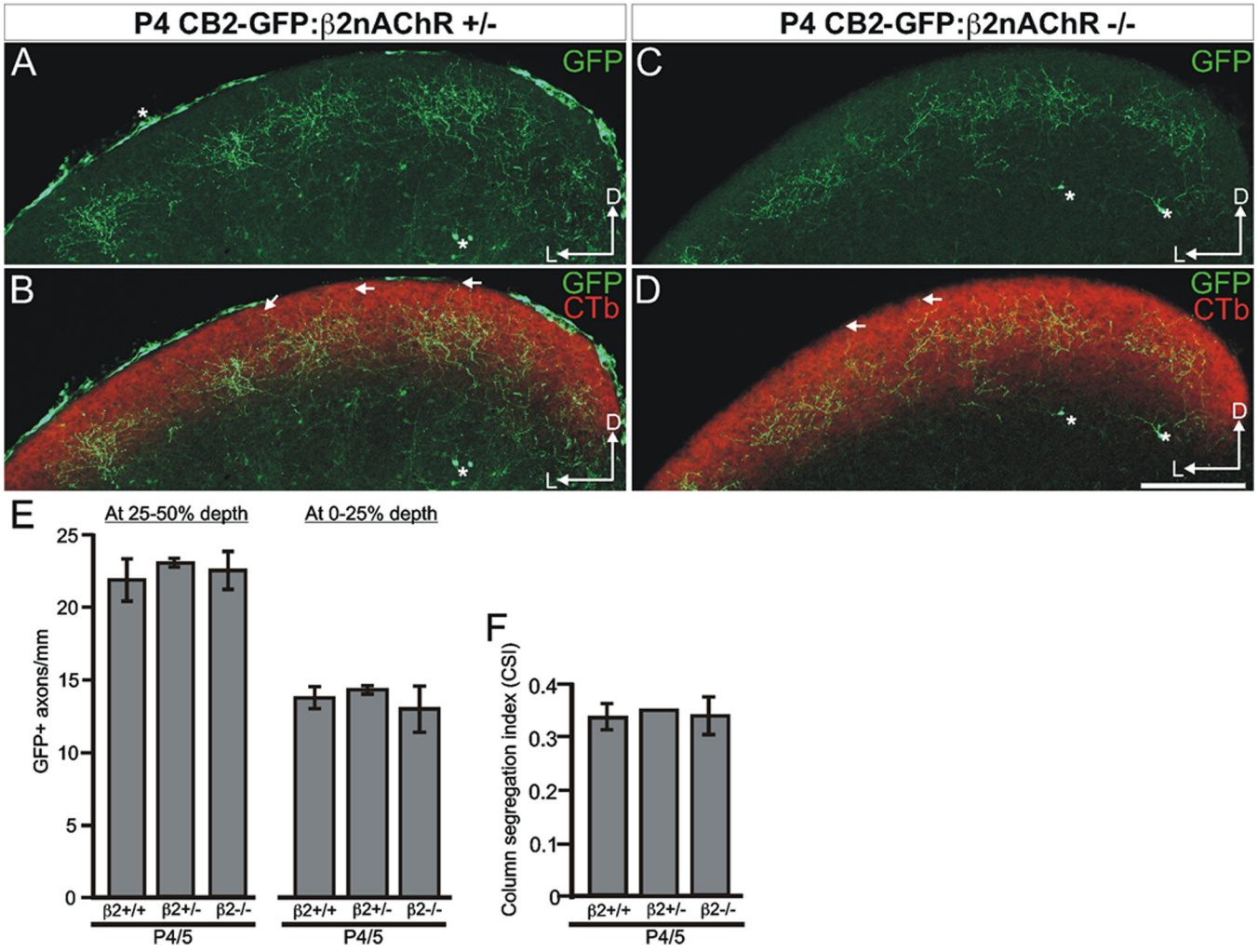

Figure 5. Genetic removal of β2nAChRs does not alter the initial targeting of tOFF-αRGC axons.

(A-D) On P4, targeting of tOFF-αRGC axons to the SC is normal in CB2-GFP:β2nAChR+/− mice and CB2-GFP:β2nAChR−/− mice. (A-D) Coronal view of the SC in a P4 CB2-GFP:β2nAChR+/− mouse (A, B), and a P4 CB2-GFP:β2nAChR−/− mouse (C, D). As in WT P4 mice (Figure 4) laminar- and columnar-specificity are not mature at this age. (A-D) Arrows indicate GFP^+ axons that project up near the pial margin. (A-D) Scale is 250 μm. (E) Quantification of laminar specificity for each genotype on P4/5; laminar specificity is indistinguishable between WT and β2nAChR+/− mice (25–50% depth, p=0.74; 0–25% depth, p=0.54), between β2nAChR+/− and β2nAChR−/− mice (25–50% depth, p=0.82; 0–25% depth, p=0.45), and between WT and β2nAChR−/− mice (25–50% depth, p=0.73; 0–25% depth, p=0.60), indicating that all genotypes start out with similar patterns of axon targeting on P4/5. (F) Quantification of columnar-specificity across genotypes on P4/5 (WT vs. β2nAChR+/−, p=0.67; β2nAChR+/− vs. β2nAChR−/−, p=0.61; WT vs. β2nAChR−/−, p=0.97).

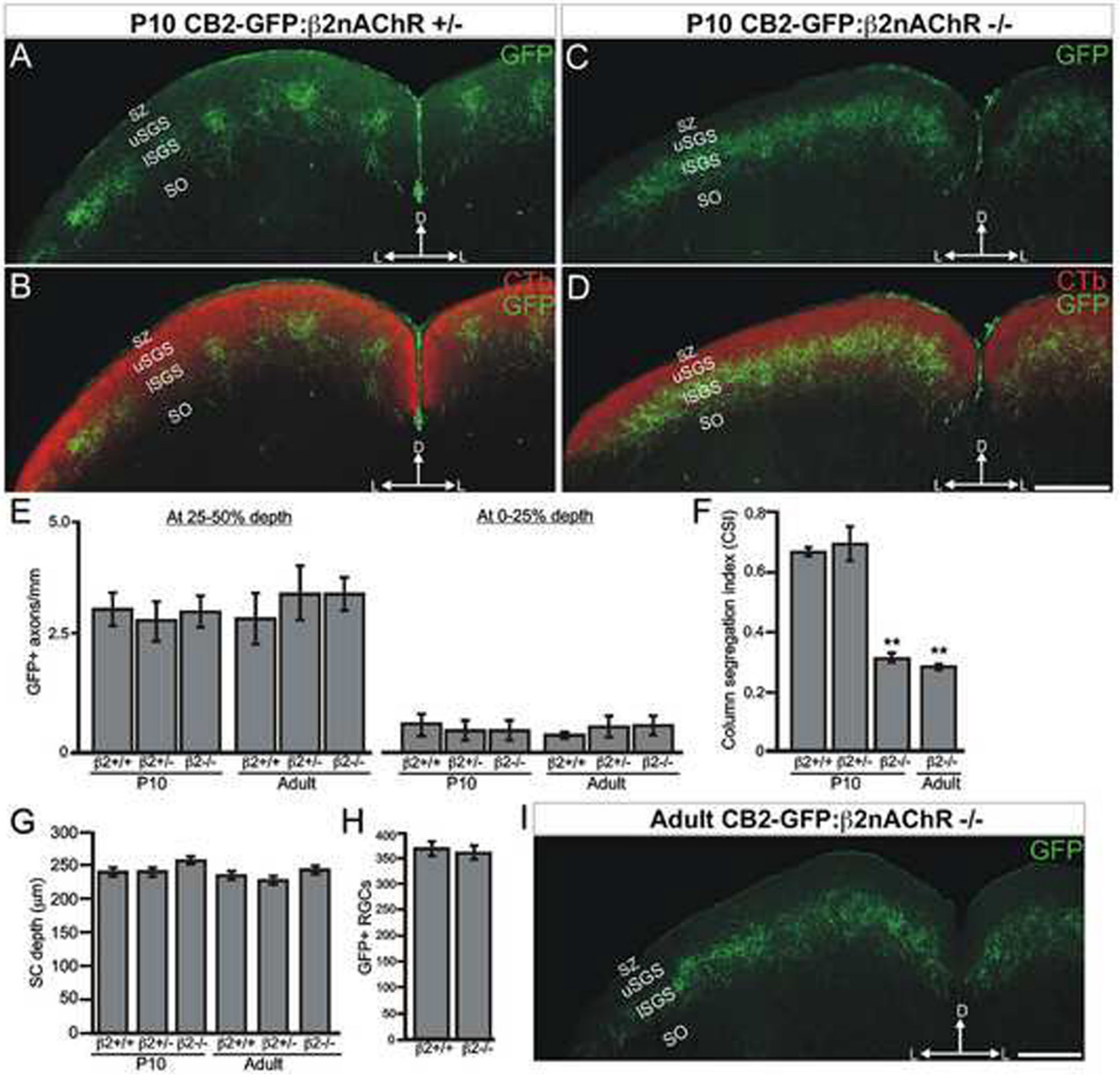

Figure 6. Cholinergic spontaneous activity mediates columnar- but not laminar-specific refinement of tOFF-αRGC projections to the SC.

(A-B) Coronal view of tOFF-αRGC projections to the SC in a P10 CB2-GFP:β2nAChR+/− mouse. Laminar-specificity and columnar specificity are similar to WT P10 mice (see Figure 4). (C, D) Coronal view of tOFF-αRGC projections to the SC in a P10 CB2-GFP:β2nAChR−/− mouse. Laminar-specificity is normal for this age but columnar specificity is severely perturbed. (A-D) Scale is 250 μm. (E) Quantification of laminar specificity according to genotype. No significant differences were present between WT, β2nAChR+/−, or β2nAChR−/− CB2-GFP mice on P10 ($p=0.3–0.7$; ±SEM; n=3 mice per condition). (F) Quantification of columnar specificity in the P10 and adult SC, according

to genotype. At P10 and at adulthood, CB2-GFP:β2nAChR−/− mice exhibit significantly less columnar-specificity than β2nAChR+/− mice or WT (β2nAChR+/+) mice (**P<0.001; n=3 mice per genotype; ±SEM; students t-test). (G) The thickness of the retinorecipient SC depth is not different between WT, β2nAChR+/− or β2nAChR−/− mice at P10 or in adulthood (p=0.2–0.5, t-test, n=3 mice per genotype). (H) The number of GFP^+ RGCs per retina is not different between WT and β2nAChR−/− CB2-GFP mice (p=0.75; t-test; ±SEM, n=4 mice per genotype). (I) GFP^+ tOFF-αRGCs projections to the SC of an adult CB2-GFP:β2nAChR−/− mouse. Columnar specificity is severely reduced (quantified in panel F). Scale is 250 μm.

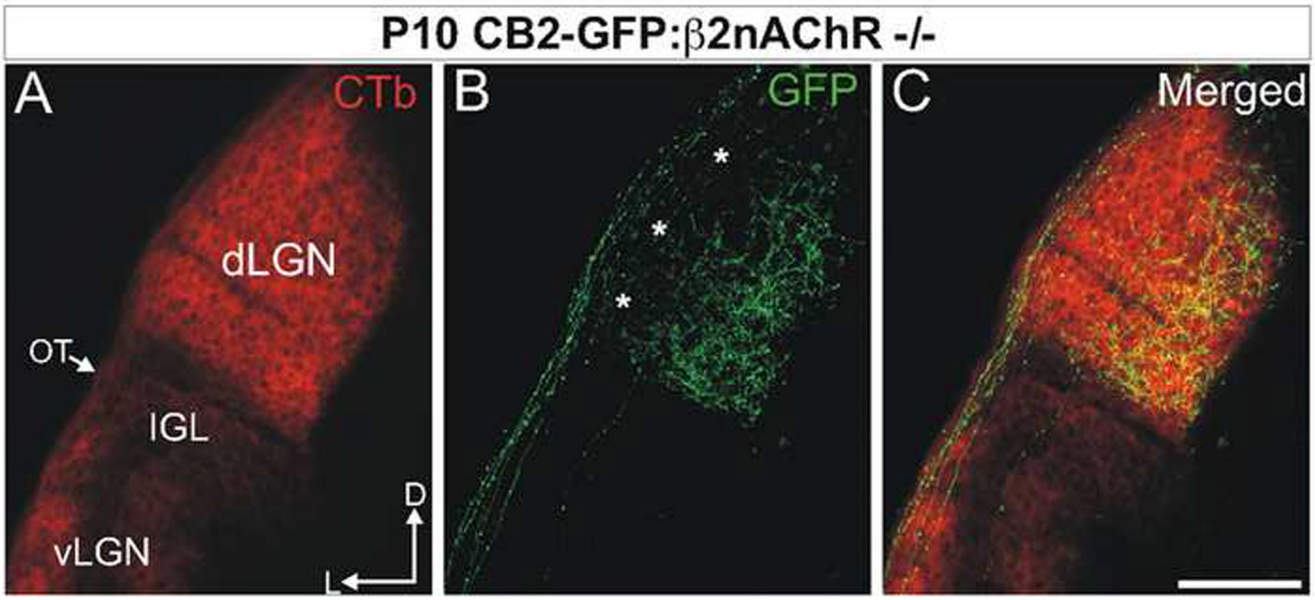

Figure 7. Disruption of cholinergic spontaneous retinal activity does not prevent laminar-specific targeting of tOFF-αRGC axons to the dLGN.

(A-C) Retino-dLGN projections in a P10 CB2-GFP:β2nAChR−/− mouse. (A) CTb-594 (red) labeled RGC retino-dLGN projections. (B) GFP^+ tOFF-αRGC axons avoid the outer third (asterisks) of the dLGN and selectively terminate within the inner portion of the dLGN, forming a distinct layer just as in WT CB2-GFP mice (see Figure 3). Note also that the GFP^+ tOFF-αRGC axons avoid the vLGN and IGL, just as in WT CB2-GFP mice. (C) Merged view of (A) and (B). Scale is 150 μm.

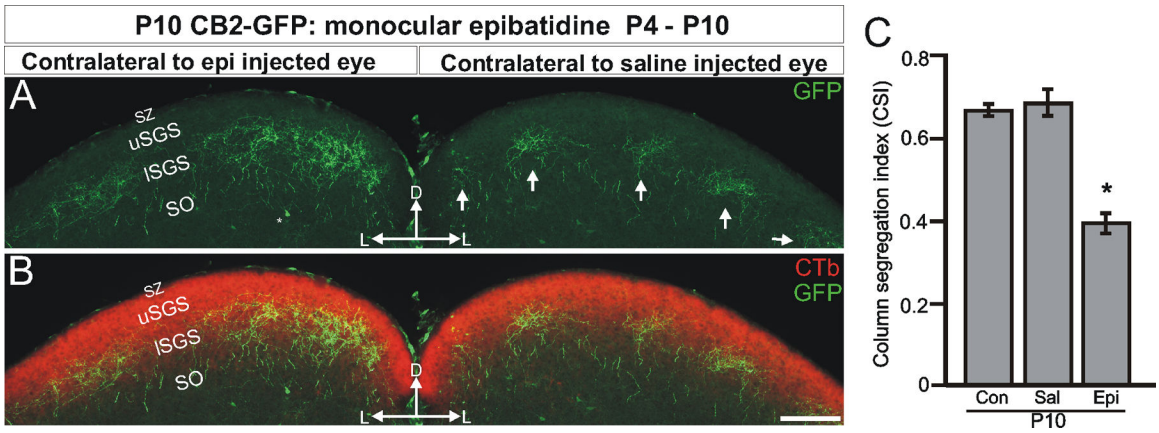

Figure 8. Columnar-specific refinement is mediated by cholinergic spontaneous activity in the retina.

(A, B) RGC projections to the SC of a P10 WT CB2-GFP mouse that received epibatidine (epi) injections into the right eye to disrupt spontaneous retinal activity and saline (control) injections into the left eye, from P4-P10. Normal laminar-specific targeting of GFP^+ tOFF-αRGC axons to the lSGS is evident in both SC hemispheres. Columnar segregation is normal in the saline hemisphere but is perturbed in the SC hemisphere contralateral to the epi-injected eye. Scale is 250 μm. (C) Quantification of columnar specificity in the SC hemisphere receiving input from control, saline- or epi-injected retina (epi vs. saline **P<0.001; saline versus control p=0.67; ±SEM; t-test; n=2 mice).